URN (Paper): urn:nbn:de:gbv:ilm1-2014iwk-118:5

58th ILMENAU SCIENTIFIC COLLOQUIUM
Technische Universität Ilmenau, 08 – 12 September 2014
URN: urn:nbn:gbv:ilm1-2014iwk:3

Tilted Wave Interferometer – Improved Measurement Uncertainty

S. Mühlig[1], J. Siepmann[1], M. Lotz[1], S. Jung[1], J. Schindler[2], and G. Baer[2]

[1] Mahr GmbH, Carl-Zeiss-Promenade 10, D-07745 Jena, Germany.
[2] Institut für Technische Optik, University of Stuttgart, Pfaffenwaldring 9, D-70569 Stuttgart, Germany.

ABSTRACT

The calibration of the tilted wave interferometer, a novel, promising and highly flexible interferometer to measure aspheres and freeform surfaces of arbitrary shape with high precision, is discussed in detail. After a short introduction of the calibration concept two different scenarios to calibrate the tilted wave interferometer are introduced. In principle, they differ in the number of applied calibration objects. One uses a single calibration sphere whereas for the second scenario multiple spheres with different radii are applied. The influence of the calibration scenarios on the measurement uncertainty of the tilted wave interferometer is revealed by virtual experiments as well as by measurements on a representative asphere.

Index Terms – Twyman-Green Interferometer, Asphere and freeform measurement, Interferometer calibration, Virtual experiments

1. INTRODUCTION

Aspheres and freeform optical surfaces promise to essentially widen the possibilities to improve and further develop high end performance optical devices. Two major aspects make the application of these special optical surfaces attractive. First, it is possible to reduce the number of optical components by using aspheres and freeform optical surfaces. This lowers production costs and reduces the weight and volume of the optical device. This is an important factor for, e.g., optics used in cell phones. Second, it is possible to lower the optical aberrations that an optical system exhibits by using aspheres and freeform surfaces. Thus, the overall performance of the entire system can be hugely enhanced.

In the present contribution a novel, promising, and highly flexible concept is discussed to measure aspheres and freeform optical surfaces of arbitrary shape with high precision and in a short time [1]. The so-called tilted wave interferometer (TWI) is based on a modified Twyman-Green interferometer. Instead of a single light source a large number of different sources are applied. Each of these light sources produces a different tilt of its wavefront in front of the surface under test (SUT). This allows measuring asphere and freeform without using a hologram. The general idea is that every single light source illuminates a part of the SUT in such a way that it locally compensates the surface normal deviation from the best fitting sphere. In other words, the illuminating rays of the light source are almost perpendicular to a local part of the SUT yielding a low line density of the resulting interferogram. In consequence, each light source allows measuring a local part of the SUT. Therefore, the combination of the interferograms of all light sources enables to measure the

entire SUT (the asphere or the freeform surface). A principle sketch of the interferometer setup can be seen in Figure 1.

The proposed concept of the TWI is very flexible and can be adapted to a wide range of different aspheres and freeform surfaces. Otherwise, the TWI constitutes a very complex optical device; the challenge is its calibration [2]. Instead of a single light source manifold different sources pass the system. Thus, the calibration of the TWI is, of course, a non-trivial task. In the present paper the calibration of the TWI is discussed in detail and optimized in order to lower the resulting measurement uncertainty. In chapter 2 the calibration concept is introduced. In the subsequent chapter 3 the influence of different calibration scenarios on the measurement uncertainty is revealed by simulations. In chapter 4 the results of the previous simulations are verified by evaluating measurements based on different calibration scenarios. Finally, the major results of this paper are concluded in chapter 5.

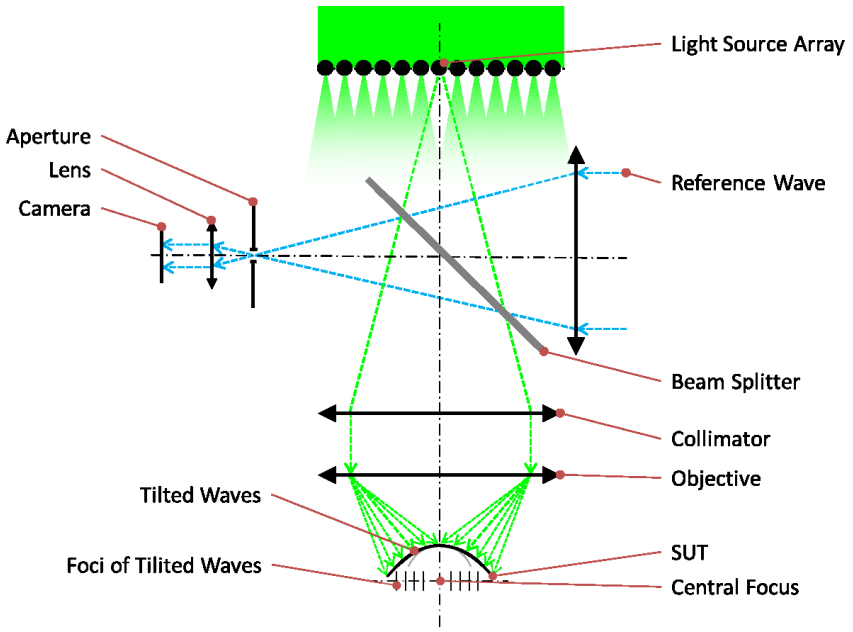

Figure 1: Principle sketch of the TWI. The different light sources of the light source array result in tilted illuminations for the SUT.

2. CALIBRATION CONCEPT

As stated previously, the calibration of the TWI is a complex task. Therefore, it cannot be entirely described here and only the major aspects are discussed. A complete description of the TWI calibration can be found elsewhere [3, 4].

Instead of a real description of the whole interferometer the TWI is treated as a black box. In other words, the propagation of the rays from the different light sources to the SUT and back from the SUT to the camera is treated in an abstract sense based on optical path lengths (OPLs). Therefore, two different areas are defined. The first one ranges from the array of light sources to the SUT and the second one from the SUT to the camera, where the interferograms are recorded.

In the first area (from the light sources to the SUT) the occurring OPLs in front of the SUT depend on four variables. The first two are the spatial coordinates of the chosen light source. The light sources are arranged onto a rectangular grid and their Cartesian coordinates are defined as M and N. The last two coordinates the OPLs depend on are the Cartesian coordinates of a chosen plane in front of the SUT where the OPLs are recorded, namely X and Y. The idea is to project the dependency of the OPLs on these four variables onto Zernike polynomials in the following sense

$$\mathrm{OPL(X,Y,M,N)} = \sum_{i,j,k,l} Q_{i,j,k,l}\, Z_{i,j,k,l}(X,Y,M,N)\,.$$

Thus, as long as the coefficients **Q** in the above equation are known every optical path length in the first area can be calculated.

The second area of the interferometer description is treated very similar to the first one. Here, the occurring OPLs depend on the Cartesian coordinates of the camera pixels, n and m, as well as on the coordinates of a chosen plane in front of the SUT, x and y. As above, this dependency is projected on Zernike polynomials yielding expansion coefficients **P**.

To sum up, if all coefficients **Q** and **P** are known, the interferometer is entirely described since every occurring OPL can be calculated. In other words, the task of the calibration is to find the **Q** and **P** coefficients that properly describe the state of the TWI.

The idea to calibrate the TWI (i.e. to find the correct **Q** and **P** coefficients) is to use calibration spheres as SUTs and measure the occurring OPLs through the entire system. The ideal interferometer, as given by the optical design, serves as a starting point. By using ray tracing algorithms the **Q** and **P** coefficients of this ideal system can be determined. Now, the **Q** and **P** coefficients of this ideal system are perturbed by small changes. For every perturbation the OPLs are calculated for the given calibration sphere. This calculation uses the perturbed **Q** and **P** matrices to describe the two areas of the TWI, as introduced above. For a given SUT only one connection between a light source and a camera pixel can be found and therewith a corresponding OPL. For every perturbation of the **Q** and **P** matrices these OPLs related to the SUT are stored in a matrix termed **A**.

By assuming a linear dependency between changes in the OPLs and changes in the **Q** and **P** coefficients, the **Q** and **P** coefficients of the real TWI setup can be found in the following way. Interferograms for the known SUT are measured and the resulting OPLs are determined. By multiplying these measured OPLs with the inverse of the matrix **A** the **Q** and **P** coefficients that describe the real state of the TWI can be found. Of course the calibration concept is only roughly summarized here and some points remain open. However, the focus of the paper is on different calibration scenarios and not on the principle concept. More details on the calibration procedure can be found elsewhere [5, 6].

3. SIMULATION OF CALIBRATION SCENARIOS

The solution of the calibration, i.e. the successful identification of the **Q** and **P** coefficients depends on various parameters. One very important one is the number of applied SUTs to measure the OPLs, as will be shown in the following.

To identify the importance of this parameter for the calibration concept two different scenarios are investigated in detail, the so-called one-sphere calibration and the multi-sphere calibration. The first one relies on a calibration of the TWI using solely one SUT. A concave calibration sphere with 10 mm radius is chosen. Manifold different combinations of sphere positions and active light sources are chosen to calibrate the TWI, as detailed below.

Only the light source in the center is activated for the first three sphere positions of the calibration sequence. The sphere is brought into the Nulltest and the Catseye position. In the following the off-centered light sources are taken into account. For every light source the sphere is brought to the position yielding an interference pattern with minimized number of oscillations. These are in principle the Nulltest positions of the sphere for the chosen light source. In the actual set up 112 off-centered light sources are applied. Finally, the sphere is brought into 15 positions in space where the incident light of manifold light sources can be detected by the camera. To sum up, for the calibration of the TWI with the chosen 10 mm radius concave sphere the calibration sequence consists of 130 different positions of the sphere in space.

The idea of the second calibration scenario is to use multiple SUTs. Therefore, it is called multi-sphere calibration. In addition to the chosen concave sphere of the one-sphere calibration (as described above) two additional spheres are applied to calibrate the TWI. The first additional sphere is a convex sphere with 15 mm radius and the second one is also convex but with a radius of 22.5 mm. Thus, the calibration sequence includes three spheres where each sphere is positioned as follows. The concave sphere is brought to the same positions as for the one-sphere calibration. Both convex spheres are placed into their Nulltest position for the central light source. Furthermore, each of the two convex spheres is brought into five different positions where multiple light sources can be detected by the camera. Therefore, the multi-sphere calibration consists of 130 positions for the concave sphere and 6 positions for each of the two convex spheres.

The performance of both calibration scenarios is compared in the following way. A virtual experiment is performed, i.e. the calibration of the TWI is simulated. Therefore, the ideal model (as given by the optical design) of the TWI is disturbed. All optical elements are allowed to be statistically rotated (the maximum is set to 0.5 °) and translated (maximum of 0.5 mm). On these perturbed models a ray tracing is performed. Thus, the **Q** and **P** coefficients of the perturbed system can be directly computed. These **Q** and **P** coefficients describe the real TWI state of this virtual experiment and are, therefore, termed $\mathbf{Q}_{\mathbf{real}}$ and $\mathbf{P}_{\mathbf{real}}$. In a perfect case the calibration procedure of the TWI should directly yield these coefficients.

The $\mathbf{Q}_{\mathbf{real}}$ and $\mathbf{P}_{\mathbf{real}}$ coefficients are applied now (together with the SUTs from the respective calibration scenario) to simulate the OPLs of the TWI. In addition, the positions of the SUTs are statistically perturbed (maximum of 1 µm). Finally, some noise is added to the simulated OPLs with maximum amplitude of 10 nm. The resulting OPLs of this procedure can be seen as an equivalent to the measured OPLs that are usually derived from the measured interferograms (see chapter 2). Therefore, these OPLs from the virtual experiment are applied as input for the normal calibration algorithm. The results of this algorithm are the **Q** and **P** coefficients of the calibration. They are termed $\mathbf{Q}_{\mathbf{calib}}$ and $\mathbf{P}_{\mathbf{calib}}$ from now on.

It is important to note, that the difference between the $\mathbf{Q}_{\mathbf{calib}}$ and $\mathbf{Q}_{\mathbf{real}}$ as well as between $\mathbf{P}_{\mathbf{calib}}$ and $\mathbf{P}_{\mathbf{real}}$ is a measure of the performance of the calibration scenario. In other words, the difference between these coefficients describes how well the calibration algorithm of the TWI

can reach the real state of the TWI setup (given by $\mathbf{Q}_{\mathbf{real}}$ and $\mathbf{P}_{\mathbf{real}}$). However, the direct comparison of these matrices is somehow cumbersome since they are polynomial expansion coefficients. Therefore, OPLs from all **Q** and **P** coefficients are generated in the respective planes in front of the SUT (see chapter 2) and from this, a characteristic OPL deviation number is calculated for each source. More precisely, this deviation number is calculated by the remaining RMS difference between the generate wavefronts, i.e the difference of wavefronts between $\mathbf{Q}_{\mathbf{calib}}$ and $\mathbf{Q}_{\mathbf{real}}$ as well as between $\mathbf{P}_{\mathbf{calib}}$ and $\mathbf{P}_{\mathbf{real}}$. The deviation quantity does not directly reflect the measurement uncertainty, but gives an estimate on the quality of the calibration, lower numbers being better. The results for the one-sphere calibration are shown in Figure 2.

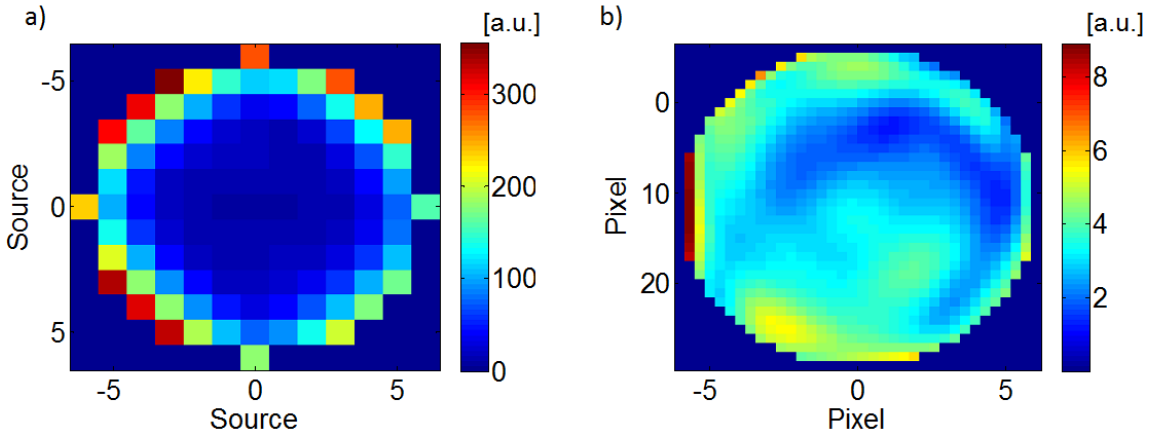

Figure 2: a) Characteristic OPL deviation numbers between $\boldsymbol{Q}_{real}$ and $\boldsymbol{Q}_{calib}$ in arbitrary units as a function of the source coordinates M and N (represented by the x- and y-axis) for the one-sphere calibration. b) Same as in a) but now the characteristic OPL deviation numbers between $\boldsymbol{P}_{real}$ and $\boldsymbol{P}_{calib}$ are shown as a function of the pixel coordinates m and n.

While for the **P** coefficients the remaining maximum characteristic OPL deviation number is around 9, which is acceptable [cf. Figure 2 b)], the one-sphere calibration yields **Q** coefficients that lead to too big deviations [cf. Figure 2 a)]. Especially, for larger source coordinates the **Q** coefficients of the calibration ($\mathbf{Q}_{\mathbf{calib}}$) cannot properly describe the real system ($\mathbf{Q}_{\mathbf{real}}$).
In Figure 3 the same comparison of the characteristic OPL deviation numbers can be seen for the multi-sphere calibration.

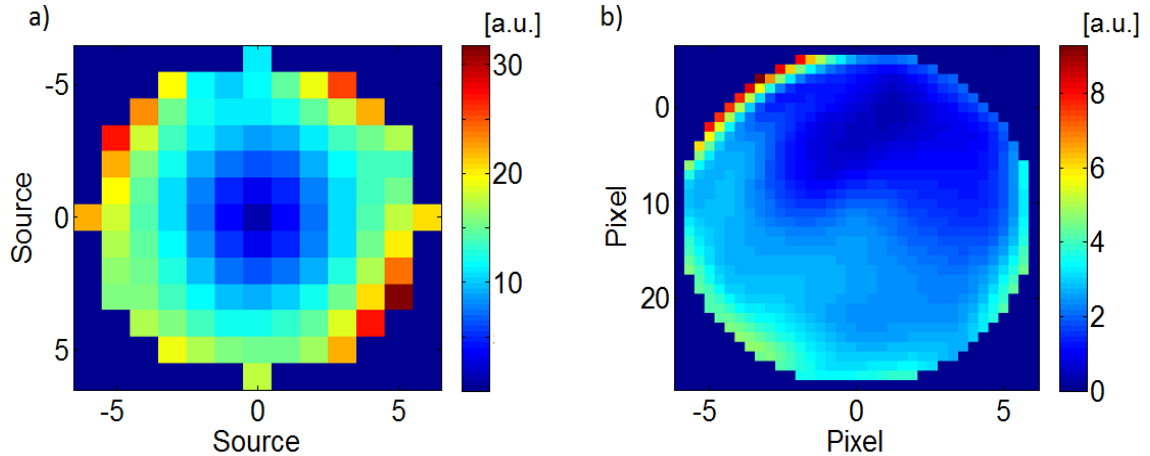

*Figure 3: Same characteristic OPL deviation numbers between **Q** and **P** coefficients of the real system and the calibration as in Figure 2, but now for the multi-sphere calibration.*

Obviously, the multi-sphere calibration yields a much smaller deviation for the **Q** coefficients compared to the one-sphere calibration [cp. Figure 2 a) and Figure 3 a)]. Using multiple spheres to calibrate the TWI reduces the characteristic OPL deviation numbers by an order of magnitude. However, an identical trend can be observed. The calibration results in higher errors for larger source coordinates. Regarding the **P** coefficients, the multi-sphere calibration yields comparable results to the one-sphere calibration.

To conclude up to this point, it has been shown by virtual experiments that using multiple spheres with different radii allow a much better calibration of the TWI. This is especially true for considering solely the **Q** coefficients. However, up to now this conclusion can be only drawn from results of the virtual experiments and the real test by measuring aspheres is missing. This is done in the next section.

4. MEASUREMENTS

The final evaluation of the two different calibration scenarios is done by measurements of a representative asphere. This asphere is measured with both calibrations of the TWI (the one-sphere and multi-sphere calibration). The results are compared to each other in Figure 4. Please note that now the calibration of the TWI is not just simulated (as in the previous chapter) but actually performed. In other words, the interferograms for all different spheres and positions and the resulting OPLs are measured.

From Figure 4 it can be clearly seen that the one-sphere calibration fails. This shows in the mismatch in the overlapping area between the measurement patches resulting from the different sources. These patch artefacts occur if the evaluation algorithm is not able to connect all the various patches (from different light sources) to a continuous surface. The failed calibration of the TWI results in systematic artefacts which are different for every patch that is detected by the camera.
From Figure 4 (right), it can be clearly seen that these patch artefacts are considerably reduced for the multi-sphere calibration, confirming the results of the simulations in section 3. Thus, using multiple objects to calibrate the TWI reduces the observed artefacts of the measured surface error.

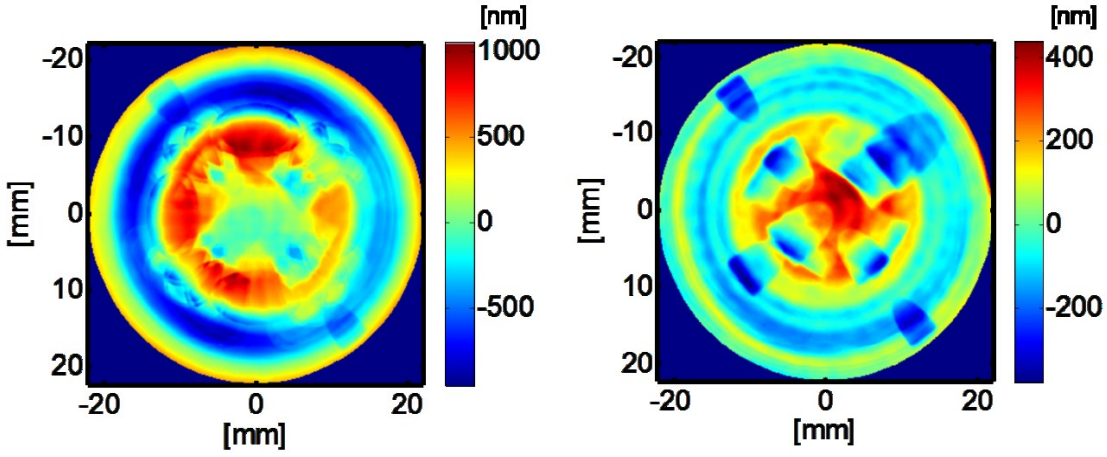

Figure 4: Measured surface errors for a representative asphere in nm. The results for the one-sphere calibration (left) as well as for the multi-sphere calibration (right) are shown. The defocus, tilt and coma term of the shown surface errors are suppressed.

Finally, the overall PV of the surface error is reduced by a factor of about two for the multi-sphere calibration in comparison to the one-sphere calibration. In other words, the measurement uncertainty can be drastically reduced for the multi-sphere calibration. Thus, the results from the previous chapter based on virtual experiments have been fully confirmed by the measurements of the asphere.

5. CONCLUSION

Two different calibration scenarios for the TWI have been introduced and discussed in detail. The first one relies on using a single calibration sphere whereas the second one uses multiple spheres with different radii. By performing virtual experiments it has been shown that the remaining error of the calibration could be drastically reduced by using multiple spheres instead of a single one. This has been confirmed by measurements on a representative asphere with the two calibration scenarios. The measurement uncertainty was considerably reduced for the multi-sphere calibration.

ACKNOWLEDGEMENTS

The work was supported by the Federal Ministry of Education and Research in the project "MesoFrei" and the European Union in the project "EURAMET IND10 Measuring optical curved surfaces". Furthermore the authors would like to thank the colleagues at the Institut für Technische Optik at the University of Stuttgart and at the Physikalisch-Technische Bundesanstalt in Braunschweig and Berlin.

REFERENCES

[1] E. Garbusi, C. Pruss, and W. Osten, "Interferometer for precise and flexible asphere testing," Opt. Lett. 33, pp. 2973-2975, 2009.
[2] C. Pruss and W. Osten, "Das Prinzip der verkippten Wellenfronten: Vorteile und Herausforderungen für die Asphärenmesstechnik," 114th conference of the DGaO, Braunschweig, p. H2, 2013.
[3] J. Liesener, E. Garbusi, C. Pruss, and W. Osten , Patent DE 10 2006 057 606 A1, 2006.
[4] E. Garbusi and W. Osten, "Perturbation methods in optics: applications to the interferometric measurement of surfaces," J. Opt. Soc. Am. A 26, pp. 2538-2549, 2009.
[5] J. Liesner, "Zum Einsatz räumlicher Lichtmodulatoren in der interferometrischen Wellenfrontmesstechnit," PhD Thesis Universität Stuttgart, 2006.
[6] G. Baer, C. Pruss, J. Siepmann, and W. Osten, "Calibration of a non-null test interferometer for the measurement of aspheres and free-form surfaces," submitted to Opt. Express, 2014.

CONTACTS

Dr. rer. nat. Stefan Mühlig stefan.muehlig@mahr.com
Dr.-Ing. Markus Lotz markus.lotz@mahr.de